Ultra-High Optical Absorption Efficiency from the Ultraviolet to the Infrared Using Multi-Walled Carbon Nanotube Ensembles

Anupama B. Kaul, James B. Coles, Michael Eastwood, Robert O. Green, and Prabhakar R. Bandaru*

The optical absorption efficiencies of vertically aligned multi-walled (MW)-carbon nanotube (CNT) ensembles are characterized in the 350–7000 nm wavelength range where CNT site densities > $1 \times 10^{11}/cm^2$ are achieved directly on metallic substrates. The site density directly impacts the optical absorption characteristics, and while high-density arrays of CNTs on electrically insulating and non-metallic substrates have been commonly reported, achieving high site-densities on metals has been challenging and remains an area of active research. These absorber ensembles are ultra-thin (<10 μm) and yet they still exhibit a reflectance as low as ~0.02%, which is 100 times lower than the reference; these characteristics make them potentially attractive for high-sensitivity and high-speed thermal detectors. In addition, the use of a plasma-enhanced chemical vapor deposition process for the synthesis of the absorbers increases the portfolio of materials that can be integrated with such absorbers due to the potential for reduced synthesis temperatures. The remarkable ruggedness of the absorbers is also demonstrated as they are exposed to high temperatures in an oxidizing ambient environment, making them well-suited for extreme thermal environments encountered in the field, potentially for solar cell applications. Finally, a phenomenological model enables the determinatiom of the extinction coefficients in these nanostructures and the results compare well with experiment.

1. Introduction

Optical absorption efficiency is an important metric for sensing, radiometric and energy harvesting applications and is intimately related to the processes and physical phenomena that occur at the nanoscale within the optically-active materials. For example, enhanced optical absorption efficiencies in hybrid polymer-nanorod materials suggests they have exceptional promise in organic solar cells,[1] while monolayer thick graphene[2] has been shown to enable solar power conversion efficiencies up to 8.6% through chemical doping.[3] Similarly, in other examples, surface plasmon modes in 50–100 nm diameter spherical, metallic nanoparticles on amorphous Si show that they scatter light more effectively which makes them attractive for solar cells.[4] In this letter, we report on another nanomaterial, an ensemble of high-density, porous arrays of thin (10–15 nm diameter), vertically oriented multi-walled carbon nanotubes (MWCNTs), which exhibits exceptional light-trapping capabilities arising from its unique physical structure. The optical-to-thermal transduction mechanism operative here offers applications for such absorbers

Dr. A. B. Kaul, J. B. Coles, M. Eastwood, R. O. Green
Jet Propulsion Laboratory
California Institute of Technology
Pasadena, CA 91109, USA
E-mail: Anupama.B.Kaul@jpl.nasa.gov
P. R. Bandaru
Jacobs School of Engineering
University of California
San Diego, La Jolla, CA 92093, USA

DOI: 10.1002/smll.201202232

NANO MICRO small

in energy harnessing, high-sensitivity thermal detectors, radiative cooling, thermography, antireflection coatings and optical baffles to reduce scattering.

Previously reported MWCNTs[5,6] and single-walled-(SW) CNTs[7] for optical absorber applications were synthesized using water-assisted thermal CVD,[8,9] which is known to yield exceptionally high growth rates with CNT lengths > 100's μm; alignment within the CNTs here occurs primarily via the crowding effect.[10,11] It is well known that thermal CVD is considered ineffective in aligning short CNTs (<10 μm). In this paper, we demonstrate that ultra-thin (10X lower compared to thermal CVD) vertically aligned CNTs are synthesized which are nonetheless 100X more absorbing than the reference. Moreover, we present optical absorption measurements on these ultra-thin, vertically aligned MWCNT ensembles well into the IR regime where it is increasingly difficult to find suitable black coatings, unlike some prior work where the focus was primarily in the visible.[5] A thin and yet highly absorbing coating with absorptance A is valuable for thermal detector applications at IR wavelengths for radiometry in order to enhance sensitivity, since the detectivity $D^* \propto A$.[12] Besides sensitivity, a thinner absorber yields high detector speeds since the thermal response time $\tau_{th} = \frac{C_{th}}{G}$, where C_{th} is the heat capacity (J/K) of the absorber, G is the thermal conductance (W/K) and $C_{th} \propto a^* l$; here a and l are the area and thickness of the absorber. Thus a >10X reduction in l has the potential to increase detector speeds by >10X.

The other structural trait for enhancing optical absorption efficiency is a high site density. Unlike the prior work on CNT optical absorbers,[5,7] where the CNTs were synthesized directly on Si or SiO_2, we demonstrate growth of high-efficiency MWCNT absorbers directly on metallic substrates where we have achieved site densities ~ $4 \times 10^{11}/cm^2$. While high density arrays of CNTs on electrically insulating and nonmetallic substrates have been commonly reported,[8,9,13] it is often desirable to grow CNTs directly on metals for lowering contact resistance in electronic devices. However, the challenges in stabilizing catalyst particles on metallic surfaces at high temperatures have generally limited CNT site densities many fold (up to 100 X). In addition, prior attempts at growing MWCNTs for optical absorber applications on substrates other than Si, such as $LiNbO_3$, yielded an absorption efficiency of ~ 85% from λ ~ 600 nm to 1800 nm,[14] whereas the CNT absorbers synthesized here on metallic substrates are shown to have an absorption efficiency > 99.98% from λ ~ 350 nm to 2500 nm. Even cermet-based materials currently used for solar selective coatings on metallic substrates such as Cu and Al,[15] have absorption efficiencies that are several orders of magnitude (up to 10^4X) lower than that reported in this paper. We also show here for the first time that the MWCNT absorbers are exceptionally rugged and exhibit a negligible change in optical absorption when exposed to temperatures as high as 400 °C in an oxidizing environment, in contrast to Au-black, a commonly used black-body reference material, which degraded considerably at much lower temperatures. Additionally, a plasma-enhanced chemical vapor deposition (PECVD) process which is used to synthesize the CNTs, increases the potential of forming these absorbers at lower synthesis temperatures compared to thermal CVD. This adds to the future prospects of integrating such absorbers with low-cost, flexible substrates for solar-cells, or with thermoelectrics for energy conversion applications, as well as fragile, temperature-sensitive micro-machined structures for IR sensing.

2. Results and Discussion

2.1. Role of Substrate and Optical Properties

The choice of the starting template was vital in synthesizing a high-density array of CNTs, which directly impacts the optical absorption characteristics. For example, the scanning-electron-microscope (SEM) image in **Figure 1**a shows amorphous carbon deposits when Co/Ti was placed directly on Si at 750 °C, exhibiting a largely reflective surface (inset of Figure 1a). On the other hand, using a Co/Ti/NbTiN template yielded a visually black sample to the naked eye (inset of Figure 1b), and the SEM image (Figure 1b) depicts a high-density array of MWCNTs which traps incoming light and suppresses reflection. The lack of growth of MWCNTs on Co/Ti/Si templates (Figure 1a) suggests that the presence of a refractory metallic nitride, such as NbTiN is important in stabilizing the catalyst nanoparticle to prevent diffusion and alloying of the catalyst with the underlying Si at high temperatures. In addition, the density of MWCNTs in the absence of the Ti layer on the Co/NbTiN templates was low. We speculate that the Ti enables the Co to fragment into nanoparticles, similar to the role of Mo in the Co-Mo bi-metallic catalyst system.[16] The Ti-Co system also appears to incorporate a larger fraction of C compared to Co alone, enhancing CNT growth.[17] Besides being of interest as absorbers in solar photo-thermal applications, the high areal density of MWCNTs on reflective, low resistivity (~110 μΩ-cm) refractory metallic nitride substrates may substantially reduce the CNT-to-substrate contact resistance which is a useful characteristic in many electronic device applications. The high magnification image in Figure 1c shows the surface of the MWCNTs arrays is rough, a factor which also contributes to scattering the incoming light diffusively. Shown in Figure 1d is the SEM image of our benchmark, a Au-black absorber, which was synthesized using approaches similar to prior reports,[18] and the percolated, random network structure of such a diffuse metal-black should be apparent.

The optical reflectance response of the CNT absorber is shown in Figure 1e, where the spectra are compared to the reference. The optical measurements were conducted from λ ~ 350 nm to 2500 nm using a high resolution, fiber coupled, spectroradiometer (ASD inc, Fieldspec Pro) where a standard white light beam was irradiated at normal incidence to the sample (schematic in inset of Figure 1e). Relative reflectance spectra were obtained by first white referencing the spectroradiometer to a 99.99% reflective spectralon panel and the reflected light intensity from the sample was then measured. The reflectance R of the CNT absorber is nearly 100X lower than that of the Au-black, e.g. ~ 0.02% at λ ~ 2000 nm compared to 1.1% for Au-black. Other commonly used absorbers, such as NiP have higher R ~ 0.5–1% for λ ~ 320–2140 nm,[19]

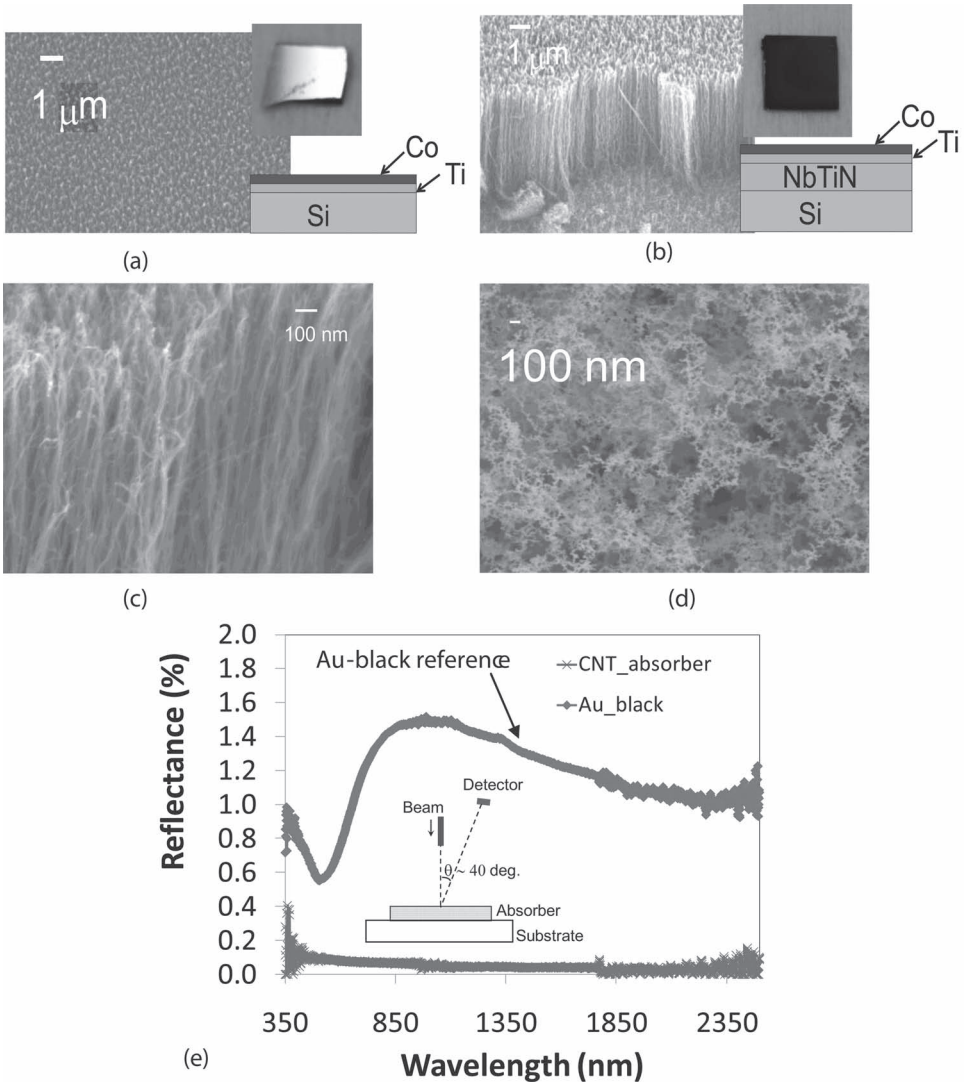

Figure 1. a) SEM micrograph of a Co/Ti/Si sample after dc PECVD growth. Top right inset shows an optical image of the sample depicting a reflective surface. (b) SEM micrograph of a Co/Ti/NbTiN sample after growth, depicting a high density carpet of MWCNTs. Top right inset shows an optical image of the sample depicting a visually black sample to the naked eye. The spatial uniformity of the MWCNT ensembles is high over large length scales. c) High magnification SEM image shows the porous, vertically aligned morphology of the CNT absorbers, in contrast to the reference benchmark Au-black absorber sample in (d) which depicts a percolated, randomly aligned network of fibers. All SEMs taken at 30° viewing angle. e) Reflectance measurement from $\lambda \sim 350$ nm–2500 nm for the MWCNT absorber and a Au-black absorber reference sample. The measurement set-up is illustrated in the bottom inset. The Au-black reference sample has $R \sim$100X larger where $R \sim 0.02\%$ for the CNT sample compared to 1.1% for the Au-black at $\lambda \sim 2000$ nm.

while ultra-black NiP alloy has $R \sim 0.16$–0.18% from $\lambda \sim$ 488–1500 nm.[20] Top-down synthesized Si nanotips exhibit $R \sim 0.09\%$ at $\lambda \sim 1000$ nm,[21] while bottom-up synthesized nanocone arrays have an absorption efficiency of ~ 93% between $\lambda \sim$ 400–650 nm.[22]

2.2. Catalyst Thickness and Modeling Analysis

The catalyst thickness impacted the optical absorption efficiency in these carbon-based nanoabsorbers significantly. Shown in **Figure 2**a are reflectance spectra taken for two samples synthesized at Co catalyst thicknesses $c \sim 5$ nm and 0.9 nm (Ti thickness fixed at 2.5 nm). The sample with $c \sim 0.9$ nm has a lower R which ranges from ~ 0.02–0.03% between $\lambda =$ 350 nm to 2500 nm, while in the sample with $c \sim 5$ nm R goes from 0.94% –0.33%. Tentatively, the decreased reflectance/increased absorption of the sample with the thinner catalyst may be expressed through an exponential decrease of the transmitted intensity $I(x)$ following a simple Lambert-Beer law formulation, i.e., $I(x) = I_o \, exp\,(-\alpha x)$, where I_o is the initial intensity of the incoming light and α is the absorption coefficient. The schematic in Figure 2b shows the geometry of the optical interrogation, as the incoming light traverses through the sparse forest of CNTs.

The typical absorption coefficient with $\alpha \sim 10^4$ cm^{-1} for $I(x = 8\ \mu m)$ is ~ 30 times the $I(x = 4.5\ \mu m)$. Now, the reflectance seems to decrease to the same order, i.e., on average

small NANO MICRO

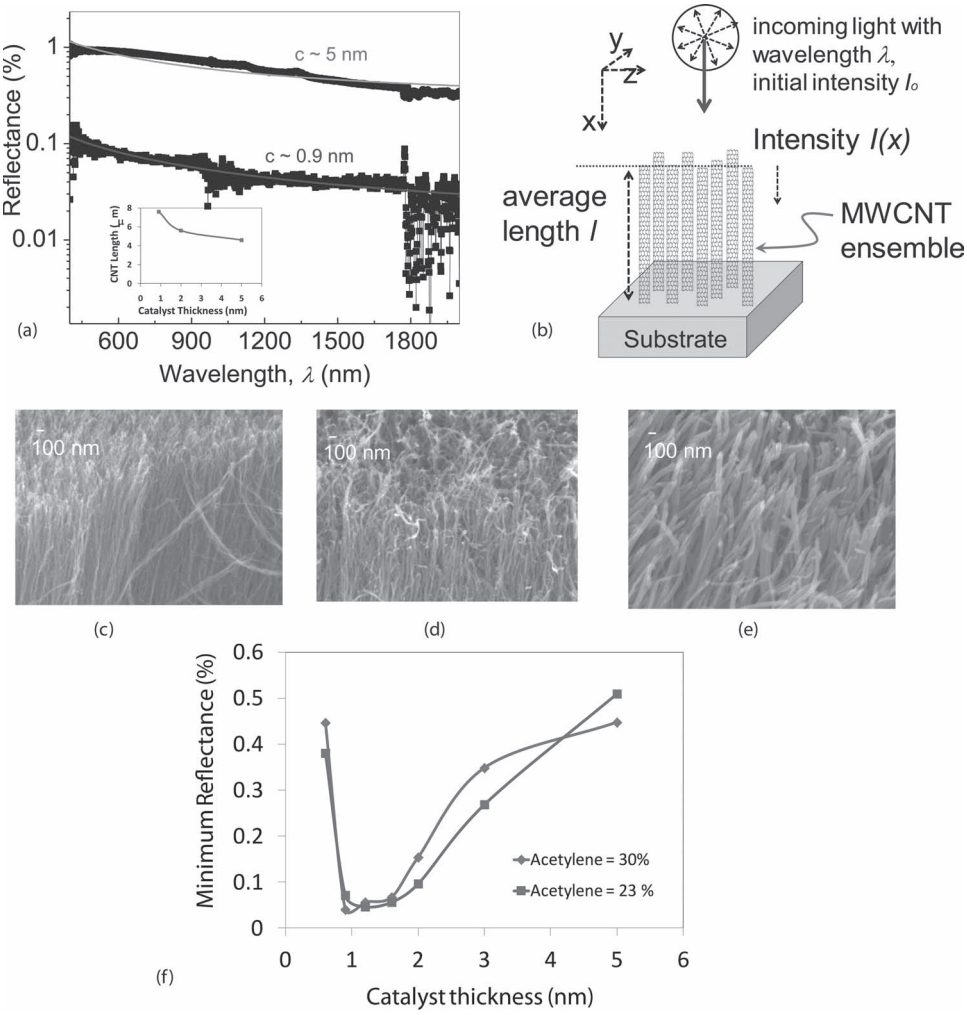

Figure 2. a) Optical reflectance spectra taken for two samples with $c \sim 0.9$ nm and 5 nm. Inset shows the variation of l with c; superimposed in the reflectance vs. wavelength data are theoretical fits from which the ratio of κ at $c \sim 0.9$ nm and 0.5 nm was determined. b) The geometry used for the optical modeling analysis. The morphology of the MWCNTs for $c \sim 0.9$ nm, 2 nm, and 5 nm is depicted in c),d) and e), respectively. In (c), thin, vertically aligned CNTs are depicted that have a high fill fraction with a site density of $\sim 4 \times 10^{11}/\text{cm}^2$ and MWCNT diameters ~ 10–15 nm, whereas in (e) the site density decreases to $\sim 6 \times 10^9/\text{cm}^2$ with MWCNT diameters ~ 80–100 nm. All SEMs taken at 30° viewing angle. f) The reflectance measurement as a function of c (taken at $\lambda \sim 1500$ nm) for two acetylene gas ratios (30% and 23%). Growth conditions in c,d and e were: 750 °C, 172 W of plasma power, 30% C_2H_2, 5 Torr.

R drops from ~0.94 to ~0.03, ~30 times as well. The SEM images of the samples with $c \sim 0.9$ nm, 2 nm and 5 nm are shown in Figure 2c, (d) and (e), respectively. This yielded a MWCNT site density of $\sim 4 \times 10^{11}/\text{cm}^2$ with MWCNT diameters $d \sim 10$–15 nm for $c \sim 0.9$, and a site density of $\sim 6 \times 10^9/\text{cm}^2$ with $d \sim 80$–100 nm for $c \sim 5$ nm. Although the length l of the MWCNTs decreased as c increased (inset of Figure 2a), with $c \sim 5$ nm, l was still > 5 μm, well above λ in these measurements, suggesting that the reduced absorption from the thicker catalyst is likely a result of changes in the fill fraction. Hence, here we have demonstrated the ability to engineer optical absorption efficiency by controlling a bottom-up parameter–the catalyst thickness–which proves to be an attractive means for tuning the optical absorption properties.

A mechanism by which porous objects suppress reflection is through a reduction in the effective refractive index n. However, porosity alone may not necessarily be the primary factor involved since the Au-black absorber sample–a largely porous structure (SEM in Figure 1d)–had higher reflectance compared to the MWCNT samples. The enhanced absorption may arise from the weak coupling of electrons in the vertically oriented CNTs to the incoming, normally-incident radiation, which back-scatter minimally, enabling light to propagate into the long pores within the arrays until it is finally absorbed. A phenomenological model for absorption was developed using a formulation where the ensembles are treated as a composite medium consisting of nanostructures and air. The intensity at any given point x in Figure 2b is given by $I(x) = I_o \exp(-\alpha x)$, where $\alpha = \frac{4\pi\kappa}{\lambda}$ and κ is the extinction coefficient. Assuming that there is no effective transmission through the substrate, $R(x) \sim (I_o - I(x))$. The corresponding variation of R with λ was then fit to $\sim a_1 e^{a_2/\lambda} + a_3$ where a_1 is related to the incident intensity I_o, a_2 is a measure of the

optical absorption length (= $\kappa \cdot l$) and a_3 is a constant. The fit to the data is shown in Figure 2a for $c \sim 0.9$ nm and 5 nm. From the fits, a_2 was determined to be ~ 0.025 and ~0.026 for $c \sim 0.9$ nm and 5 nm, respectively, and given that the ratio, $\frac{(a_2)_{0.9}}{(a_2)_5} = \frac{(\kappa \cdot l)_{0.9}}{(\kappa \cdot l)_5}$ and that l is 8 μm and 5 μm, respectively, we obtain a ratio of the extinction coefficients, $\frac{\kappa_{0.9}}{\kappa_5}$ of ~ 0.6.

We rationalize such a value by appealing to the relationship of the complex refractive index, $\tilde{N}$ (= $n + i\kappa$) to the dielectric constant, $\sqrt{\tilde{\varepsilon}}$ (where, $\tilde{\varepsilon} = \varepsilon_1 + i\,\varepsilon_2$).[23] It can then be derived that when absorption dominates, κ is proportional to $\sqrt{\tilde{\varepsilon}}$. Using a simple rule of mixtures, the dielectric constant of the air-CNT mixture, $\tilde{\varepsilon} = \alpha \cdot \varepsilon_{CNT} + \beta \cdot \varepsilon_{air}$, where α and β are the fractions of the CNT and air, respectively (*i.e.* $\alpha + \beta = 1$).[24] For the observed MWCNT site density of ~ 4×10^{11}/cm^2 for $c \sim 0.9$ nm, an average area per MWCNT is determined to be ~ 250 nm^2. Now, with an average $d \sim 10$ nm, the area fraction α is ~ 0.31, where it is assumed that all the MWCNTs are perpendicular to the incident radiation. For the samples with $c \sim 5$ nm, site density ~ 6×10^9/cm^2 and average $d \sim 100$ nm, the corresponding average area per MWCNT is ~ 0.16×10^4 nm^2, and α is ~ 0.47. We use an average dielectric constant, $\tilde{\varepsilon}$ of ~ 23 for the CNTs over λ = 350–3100 nm, extrapolated from the values of the complex refractive index of graphite[25] at $\lambda \sim 350$ nm and 3100 nm, respectively. Since $\kappa \sim \sqrt{\tilde{\varepsilon}}$ we compute the ratio $\frac{\kappa_{0.9}}{\kappa_5} \sim \sqrt{\left(\frac{(0.31 \cdot 23) + (0.69 \cdot 1)}{(0.47 \cdot 23) + (0.53 \cdot 1)}\right)} \sim 0.8$. The value of the $\frac{\kappa_{0.9}}{\kappa_5}$ ratio is then found to be quite close to the value obtained by the fitting shown in Figure 2a.

It is interesting that κ is smaller for the MWCNTs grown with $c \sim 0.9$ nm compared to CNTs grown with $c \sim 5$ nm. This observation can be rationalized on the basis of a smaller area fraction in the former case, i.e., 0.31 vs. 0.47. While such a rationalization does not explicitly consider the volume absorption due to a larger l in the former case (i.e., 8 μm *vs.* 5 μm), it is justified since it has previously been shown that for the case of absorption in Si nanowires[26] the absorption in a thin film over a wide energy range comparable to the one used in the present work, is on the average equivalent to the absorption in the nanowires. The larger absolute magnitude of R for the sample with $c \sim 5$ nm compared to the sample with $c \sim 0.9$ nm may indicate an influence of the substrate in the latter, the effect of which is more pronounced due to a shorter l for $c \sim 5$ nm.

A more detailed analysis of the impact of catalyst thickness on the optical reflectance properties of the MWCNT absorbers was conducted for a wide range of catalyst thicknesses (Figure 2f). This data (at $\lambda \sim$ 1500 nm) shows a minimum of R at $c \sim$ 1 nm. However, R increases when $c \sim 0.6$ nm due to the inability to nucleate a high enough areal density of MWCNTs; such behavior was consistent for two different acetylene gas concentrations, as indicated.

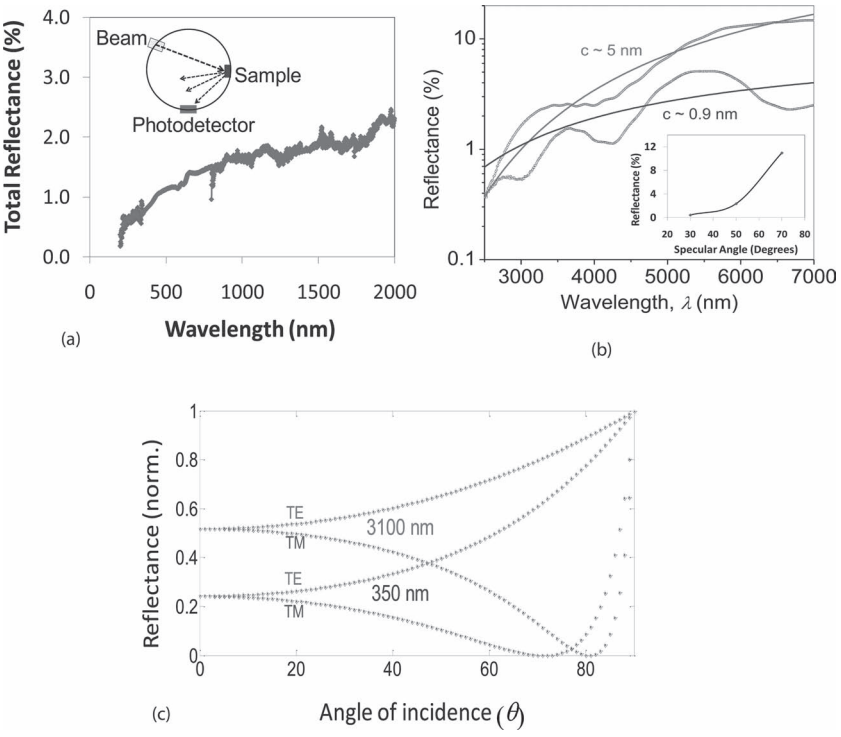

Figure 3. a) Total hemispherical reflectance measurements made from $\lambda \sim$ 250 nm–2000 nm reveals $R_T \sim 1.8\%$ at 1000 nm. Inset shows a schematic of the measurement set-up. b) Long-wavelength IR measurements, which yields $R \sim 2.4\%$ for the sample with $c \sim 0.9$ nm, while $R \sim 14.7\%$ for $c \sim 5$ nm at $\lambda \sim 7000$ nm. Superimposed is a theoretical fit to the data for $c \sim 0.9$ nm and 5 nm. The undulations in the reflectance are possibly due to interference effects from the substrate. Growth conditions: 750 °C, 170 W of plasma power, 30% C_2H_2, and 5 Torr. Inset shows the angular dependence where R is fairly low ~ 2% up to 50°, and a small increase up to ~ 10% is seen at 70°. c) The variation of R with specular angle of incidence, assuming TE and TM polarized-modes of radiation. While a polarization-sensitive study can yield additional insights, an absolute minima in the TM mode at 72° can be used to completely suppress R.

2.3. Total Reflectance and Long Wavelength IR Response

In **Figure 3**a, the data for the total reflectance R_T of the CNT samples, measured using an integrating sphere (schematic in inset of Figure 3a), indicates an $R_T \sim 1.8\%$ at $\lambda \sim 1000$ nm. This is more than 4 X lower than top-down synthesized Si nanotips with an $R_T \sim 8\%$ at $\lambda \sim 1000$ nm.[21] In addition, R_T of our samples is 0.8% at $\lambda \sim 400$ nm, in contrast to Si nanostructured films which have $R_T \sim 1.46\%$ in the range of $\lambda \sim$ 300–600 nm.[27] Optical reflectance measurements on the CNT absorbers were also extended to the longer IR wavelengths, where it is increasingly difficult to find highly efficient optically black coatings. Shown in Figure 3b is the specular reflectance, measured using a Harrick 30° specular reflectance attachment, for samples with $c \sim 0.9$ nm and 1.6 nm. Again, the specular reflectance for samples with the thinner catalyst $c \sim 0.9$ nm was much lower (~2.4%) than CNTs grown with $c \sim$1.6 nm (~14.7%) at $\lambda \sim 7000$ nm; this confirms the

NANO MICRO small

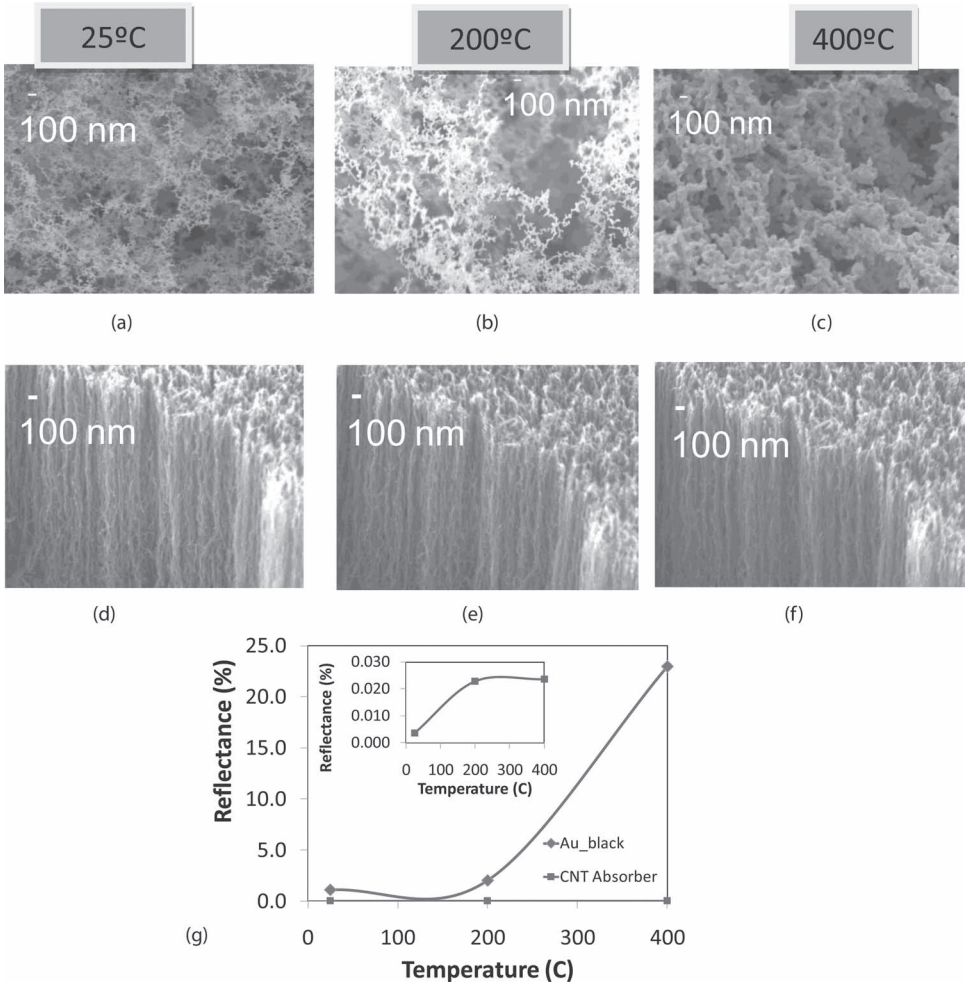

Figure 4. SEM images in (a)–(c) correspond to thermal tests conducted on Au-black absorber samples. The Au-black absorber sample at a) 25 °C, after heating to b) 200 °C, and c) 400 °C for 1 hour in air. After heating to 200 °C, the percolated structure of the Au-black absorber sample appears to fragment as shown in (b), and at 400 °C the structure collapses completely (c) as the filaments coarsen. SEM images in (d)–(f) correspond to thermal tests conducted on the CNT absorber samples. The CNT absorber sample at d) 25 °C, after heating to e) 200 °C, and f) 400 °C. The MWCNT absorbers have a high structural integrity since no change in morphology is detected after heating to 200 °C (e) and 400 °C (f). All SEMs taken at 30° viewing angle. (g) Shown is *R* of the Au-black and CNT absorber samples as a function of temperature. The Au-black absorber shows *R* increases up to 23% after heating to 400 °C. The inset shows *R* (CNT sample) increases slightly after exposure to 200 °C but it is still very low, ~ 0.022% at $\lambda \sim 2000$ nm; it remains unchanged after exposure to temperatures as high as ~ 400 °C.

highly absorbing characteristic of these absorbers at long IR wavelengths.

The angular dependence of the specular reflectance was also measured in the range of 30° to 70°, as shown in the inset of Figure 3b (taken at $\lambda \sim 2500$ nm). Although the intensity of the specular reflectance increases with incident angle, the change is relatively small. In comparison, other anti-reflection thin film coatings suppress reflection over a narrow band of angles and have selective absorption characteristics over a narrow spectral range.

Modeling analysis was also pursued at longer wavelengths (>2500 nm) where the increase in R was fit to an expression of the form, $R(\lambda) = R_o \exp(-\alpha/\lambda)$ and the fits to the data are shown in Figure 3b. It was found from the fits that the value of α for $c \sim 0.9$ nm and 5 nm was ~ 12560 nm and ~6850 nm, respectively. From the ratio $\frac{(\alpha)_{0.9}}{(\alpha)_5} = \frac{(\kappa \cdot l)_{0.9}}{(\kappa \cdot l)_5}$ we deduce a $\frac{\kappa_{0.9}}{\kappa_5}$ value of ~0.4, which is again close to the previously determined ratio.

The angular dependence of R can be modeled by assuming that the incident radiation is predominantly Transverse Electric (TE) polarized; experimentally, it is possible that the beam is more polarized in one mode than the other but more thorough measurements need to be conducted to quantify this more accurately. It was seen from Figure 3c, that R increases with angle, as seen for the TE polarization and also that the absolute magnitude of R increases with λ, confirming our experimental observations as well. In the future, polarization-sensitive measurements will be undertaken, for example with the Transverse Magnetic (TM) optical mode as well, where the E-field is along the axis of the CNTs, and greater absorption is expected. This would yield a minimum in R at a specific angle, for example at ~ 72° with $\lambda = 350$ nm

as shown in Figure 3c, which may be used in completely supressing *R*.

2.4. Thermal Ruggedness

We now present data which demonstrates the exceptionally low *R* of the MWCNT absorbers even after they were exposed to temperatures as high as 400 °C in air under an oxidizing environment, as might be expected with incident solar radiation. In comparison, the structural characteristics of the Au-black absorber reference gradually deteriorates with increasing temperature, as indicated by the SEM images of **Figures 4**a–c. However, the structural characteristics of the MWCNT absorber samples are largely unchanged when heated from 25 °C (Figure 4d), to 200 °C (Figure 4e) and to 400 °C (Figure 4f).

From the corresponding optical spectra (Figure 4g) it is apparent that *R* of the Au-black absorber sample increases as it is heated from 25 °C to 200 °C (2%) and is ~ 23% at 400 °C (at λ ~2000 nm). On the other hand, the *R* of the CNT absorbers is still very low, ~ 0.022% after heating to 200 °C (inset of Figure 4g), and remains unchanged after exposure to temperatures as high as 400 °C which can be correlated to the structural integrity of the CNT absorbers to temperatures as high as 400 °C (Figure 4f). Since amorphous carbon burns at temperatures as low as 200 °C in an oxidizing environment, the fact that there is negligible change in optical properties as the samples are heated to 400 °C (Figure 4g), suggests that our PECVD synthesized CNTs are of high quality.

3. Conclusion

In conclusion, we have successfully shown that PECVD synthesized MWCNTs yield a high site-density directly on metallic substrates which exhibit ultra-low reflectance (~0.02%) over a wide spectral range from UV-to-IR for relatively thin (<10 μm) absorber ensembles. Their highly-efficient optical absorption properties and exceptional ruggedness at high temperatures suggests their promise in solar photo-thermal applications and IR thermal detectors for radiometry applications. In addition, the use of a plasma-based process increases the potential for synthesizing the absorbers at lower temperatures in the future. This increases the likelihood of integrating the absorbers with low-cost flexible substrates, potentially for solar-cell applications, as well as thermoelectrics and micro-machined structures for enabling new classes of IR sensors that could potentially operate in rugged environments.

4. Experimental Section

The initial substrate for the synthesis of the MWCNTs was a <100> oriented Si wafer on which a 100–200 nm thick layer of a refractory metallic nitride, NbTiN with resistivity ρ ~ 110 $\mu\Omega$-*cm*, was deposited reactively using dc magnetron sputtering. Bi-metallic layers of Co (thickness range 0.6 nm –6 nm) and 2.5 nm thick Ti were e-beam evaporated and served as the catalyst. Beside the Co/Ti/NbTiN/Si templates, control samples of Co/Ti/Si, Co/NbTiN/Si and Co/Si were also prepared. Multiple samples (area ~4 cm^2) were placed on a wafer during PECVD growth so that a comparative analysis could be performed. At temperatures in the range of 550 to 750 °C, H_2 was flowed into the chamber for several minutes, and the growth gases acetylene (C_2H_2) and ammonia (NH_3) were then introduced to a typical pressure of ~5 Torr and the discharge was then ignited.

Acknowledgements

We thank K. Megerian, M. Anderson, and R. Kowalczyk for technical assistance and T. Pagano, P. Goldsmith, J. Hyon, M. Foote, and W. Holmes for useful discussions. This research was carried out at the Jet Propulsion Laboratory, California Institute of Technology, under a contract with the National Aeronautics and Space Administration and was funded through the internal Research and Technology Development (R&TD) program (01STCR, R.10.021.067). ABK also acknowledges support for this work through the National Science Foundation's IR/D program.

[1] J. Weickert, R. B. Dunbar, H. C. Hesse, W. Wiedemann, L. Schmidt-Mende, *Adv. Mater.* **2011**, *23*, 1810.
[2] R. R. Nair, P. Blake, A. N. Grigorenko, K. S. Novoselov, T. J. Booth, T. Stauber, N. M. R. Peres, A. K. Geim, *Science* **2008**, *320*, 1308.
[3] X. Mao, S. Tongay, M. Petterson, K. Berke, A. Rinzler, B. R. Appleton, A. F. Hebard, *Nano Lett.* **2012**, *12*, 2745.
[4] D. Derkacs, S. H. Lim, P. Matheu, W. Mar, E. T. Yu, *Appl. Phys. Lett.* **2006**, *89*, 093103.
[5] Z-P. Yang, L. Ci, J. A. Bur, S-Y. Lin, P. M. Ajayan, *Nano Lett.* **2008**, *8*, 446.
[6] Z-P. Yang, M-L. Hsieh, J. A. Bur, L. Ci, L. M. Hanssen, B. Wilthan, P. M. Ajayan, S-Y. Lin, *Appl. Optics* **2011**, *50*, 1851.
[7] K. Mizuno, J. Ishii, H. Kishida, Y. Hayamizu, S. Yasuda, D. N. Futaba, M. Yumura, K. Hata, *Proc. Natl. Acad. Sci. USA* **2009**, *106*, 6044.
[8] K. Hata, D. N. Futaba, K. Mizuno, T. Namai, M. Yumura, S. Iijima, *Science* **2004**, *306*, 1362.
[9] T. Yamada, T. Namai, K. Haa, D. N. Futaba, K. Mizuno, J. Fan, M. Yudasaka, M. Yumura, S. Iijima, *Nat. Nanotechnol.* **2006**, *1*, 131.
[10] S. Fan, M. G. Chapline, N. R. Franklin, T. W. Tombler, A. M. Cassell, H. Dai, *Science* **1999**, *283*, 512.
[11] R. Andrews, D. Jacques, A. M. Rao, F. Derbyshire, D. Qian, X. Fan, E. C. Dickey, J. Chen, *Chem. Phys. Lett.* **1999**, *303*, 467.
[12] P. Eriksson, J. Y. Andersson, G. Stemme, *Physica Scripta* **1994**, *T54*, 165.
[13] G. D. Nessim, A. J. Hart, J. S. Kim, D. Acquaviva, J. M. Oh, C. D. Morgan, M. Seita, J. S. Leib, C. V. Thompson, *Nano Lett.* **2008**, *8*, 3587.
[14] J. H. Lehman, R. Deshpande, P. Rice, B. To, A. C. Dillon, *Infrared Phys. and Tech.* **2006**, *47*, 246.
[15] C. Nunes, V. Teixeira, M. Collares-Pereira, A. Monteiro, E. Roman, J. Martin-Gago, *Vacuum* **2002**, *67*, 623.
[16] Y. Murakami, S. Chiashi, Y. Miyauchi, S. Maruyama, *Jpn. J. Appl. Phys.* **2004**, *43*, 1221.

[17] S. Sato, A. Kawabata, D. Kondo, M. Nihei, Y. Awano, *Chem. Phys. Lett.* **2005**, *402*, 149.
[18] D. J. Advena, V. T. Bly, J. T. Cox, *Appl. Opt.* **1993**, *32*, 1136.
[19] C. E. Johnson, *Metal Finish.* **1980**, *78*, 21.
[20] S. Kodama, M. Horiuchi, T. Kuni, K. Kuroda, *IEEE Trans. Inst. and Meas.* **1990**, *39*, 230.
[21] C. Lee, S. Bae, S. Mobasser, H. Manohara, *Nano Lett.* **2005**, *5*, 2438.
[22] J. Zhu, Z. Yu, G. F. Burkhard, C.-M Hsu, S. T. Connor, Y. Xu, Q. Wang, M. McGehee, S. Fan, Y. Cui, *Nano Lett.* **2009**, *9*, 279.
[23] M. Fox, *Optical Properties of Solids*, Oxford University Press, New York, NY **2001**.
[24] A. Arriagada, E. T. Yu, P. R. Bandaru, *J. Thermal Anal. Calorimetry* **2009**, *97*, 1023.
[25] T. de Los Arcos, P. Oelhafen, D. Mathys, *Nanotechnology* **2007**, *18*, 265706.
[26] L. Hu, G. Chen, *Nano Lett.* **2007**, *7*, 3249.
[27] K. Peng, Y. Wu, H. Fang, X. Zhong, Y. Xu, J. Zhu, *Angew. Chem. Int. Ed.* **2005**, *44*, 2737.

Received: September 10, 2012
Published online: December 11, 2012

